Single Nanowire OPV Properties of a Fullerene-Capped P3HT Dyad Investigated Using Conductive and Photoconductive AFM

Daniel A. Kamkar, Mingfeng Wang, Fred Wudl,* and Thuc-Quyen Nguyen*

Center for Polymers and Organic Solids and Department of Chemistry & Biochemistry, University of California, Santa Barbara, California 93106, United States.

ABSTRACT

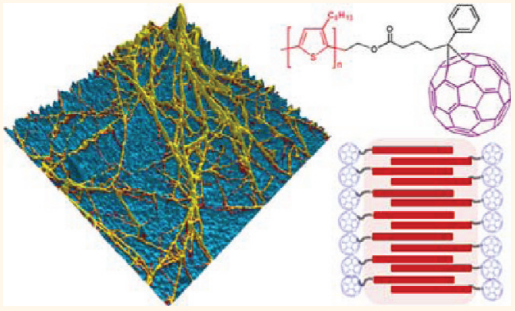

The effect of molecular self-assembly on nanoscale photoinduced charge generation of fullerene-capped poly(3-hexylthiophene) (PCB-c-P3HT) films and its effectiveness as a molecular additive in bulk heterojunction P3HT:[6,6]-phenyl-C_{61}-butyric acid methyl ester (PCBM) is investigated through photoconductive atomic force microscopy. *ortho*-Dichlorobenzene-cast films of PCB-c-P3HT are found to form interconnected fibrous networks that show high photocurrent generation, while tetrahydrofuran-cast films show nanospheres with relatively low photocurrent generation. The nanofiber size and current generated from these nanowires are shown to vary with additions of PCBM. The PCB-c-P3HT amphiphile is shown to be a successful molecular additive in P3HT:PCBM films. These observations demonstrate how the self-assembly of PCB-c-P3HT into specific nanostructures is crucial to charge generation and transport.

KEYWORDS: bulk heterojunction photovoltaic · nanowires · photocurrent · conductive AFM · photoconductive AFM · fullerene · poly(3-hexylthiophene) · self-assembly

There has been extensive research in recent years to develop organic bulk heterojunction (BHJ) photovoltaic technology because of its potential application as an inexpensive and lightweight energy source.[1−3] An important strategy for increasing the efficiency of BHJ photovoltaics is controlling the nanoscale morphology of the active layer. There are ways to modify the BHJ morphology including concentration and ratio of the donor and acceptor in solution, choice of solvent, casting methods,[4] thermal annealing,[5] solvent additives,[6−8] and molecular additives.[9−17] To investigate the effect these processing conditions have on the active layer morphology, a variety of techniques have been used including X-ray diffraction (XRD),[18−20] transmission electron microscopy (TEM),[6,21] scanning electron microscopy (SEM),[22,23] and scanning tunneling microscopy (STM).[24] In addition to these techniques, various forms of scanning probe microscopy are used to investigate nanoscale morphology such as tapping mode atomic force microscopy (t-AFM),[25−30] electrostatic force microscopy (EFM),[31,32] scanning kelvin probe microscopy (SKPM),[32−34] as well as conductive AFM (c-AFM)[5,9,35−37] and photoconductive AFM (pc-AFM).[5,38−44]

One of the most widely studied BHJ systems in terms of nanoscale morphology is poly(3-hexylthiophene) (P3HT) as the electron donor and [6,6]-phenyl-C_{61}-butyric acid methyl ester (PCBM) as the electron acceptor.[4,45−47] When blended with PCBM under certain processing conditions, such as thermal annealing or choice of solvent, P3HT fibers can form. However, thermal annealing can cause large-scale phase separation or crystalline PCBM domain formation. Thus, controlling the self-assembly of conjugated polymers *via* chemical modification is desirable. To this end, these two functional units have been incorporated into a dyad designed to serve as a molecular additive for the highly optimized P3HT:PCBM system.[48]

Recently, we found that capping a P3HT chain with PCBM, PCB-c-P3HT (Figure 1a), leads to well-defined nanostructure formation where the solvent plays a vital role in determining the morphology and nanostructures

* Address correspondence to quyen@chem.ucsb.edu, wudl@chem.ucsb.edu.

Received for review September 30, 2011 and accepted January 12, 2012.

Published online January 20, 2012
10.1021/nn204565h

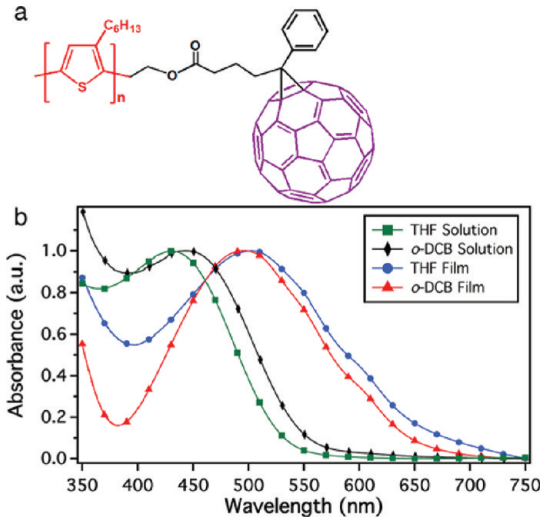

Figure 1. (a) Chemical structure and (b) normalized UV−vis spectra of PCB-c-P3HT solutions and films: THF (green squares) and *o*-DCB (black diamonds) solutions and THF- (blue circles) and *o*-DCB-cast films (red triangles).

formed.[49] PCB-c-P3HT films cast from a tetrahydrofuran (THF) solution were found to form spherical aggregates, while PCB-c-P3HT films cast from an *ortho*-dichlorobenzene (*o*-DCB) solution were found to form nanowires as long as micrometers with a diameter of 15−20 nm. It has been suggested in previous work[49] that, in PCB-c-P3HT solutions cast from THF, the methanofullerene moieties aggregate into a micelle core and are stabilized by P3HT chains that extend to the solvent medium, while in the fibrous PCB-c-P3HT structures cast from *o*-DCB, P3HT chains crystallize to form a core which is surrounded by a monolayer of C_{61} moieties. These different self-assembling structures of the PCB-c-P3HT provide an interesting model system to study the relationship between photoinduced charge transfer and nanoscale morphology at well-defined fullerene/polymer interfaces. Herein, we utilize c-AFM and pc-AFM to study the nanoscale photoinduced charge generation in two distinct self-assembled nanostructures of PCB-c-P3HT films: *nanospheres* and *nanowires*. Our results clearly indicate that the charge generation is strongly dependent on the self-assembly of PCB-c-P3HT such that the nanowires of PCB-c-P3HT show dramatically higher short-circuit photocurrent than the nanospheres under the same conditions.

RESULTS AND DISCUSSION

In a P3HT:PCBM BHJ, when an exciton separates into mobile carriers, holes and electrons remain in the P3HT and PCBM, respectively. The free carriers can travel through percolated pathways to be collected by their respective electrodes: holes are collected by the anode, and electrons are collected by the cathode.[38] In this PCB-c-P3HT system, it is reasonable to expect that holes travel through the P3HT segments while electrons travel through the PCB segments of the dyad.

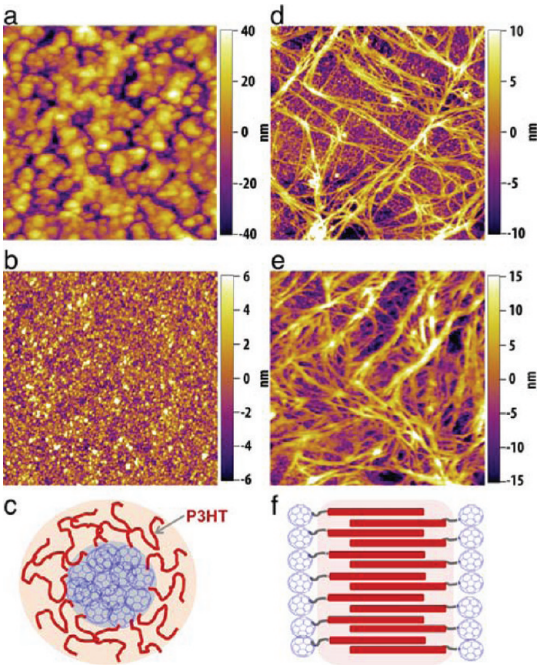

Figure 2. Surface topographic images and schematic drawings of proposed molecular self-assembled models of PCB-c-P3HT prepared from THF (a−c) and *o*-DCB solutions (d−f) casted onto Si/SiO_2 (a,d) and APTMS-ITO (b,e). Image sizes are 5 μm × 5 μm.

Normalized absorption spectra of solutions and films are shown in Figure 1b. The THF solution shows an absorption peak around 430 nm, while *o*-DCB solution shows an absorption peak at 445 nm. This difference in the absorption peak is a result of different polymer chain conformation in solution as has been observed for other conjugated polymers.[50,51] The more extended chain conformation of PCB-c-P3HT in *o*-DCB solution leads to a longer absorption wavelength onset. When the films are cast onto cleaned indium tin oxide (ITO), this absorption peak is significantly red-shifted for films cast from both solutions. The peak for the THF-cast film shifts from 430 to 500 nm, and the peak for the *o*-DCB-cast film shifts from 445 to 495 nm. Both films also show a small shoulder at 550 nm. These absorption spectra are similar to the absorption spectra of P3HT:PCBM blends as well as polythiophene-based diblock copolymers with a fullerene block attached.[52]

Tapping mode AFM images of THF- and *o*-DCB-cast films were collected to examine the impact of substrate and solvent on the film morphology (Figure 2). In all THF-cast films, nanospheres are observed (Figure 2a,b), while *o*-DCB-cast films show interconnected wire networks (Figure 2d,e), absent in THF-cast films. However, the sizes of nanospheres and fibers depend on underlying substrates. Nanospheres on silicon/silicon dioxide (Si/SiO_2) and aminopropyltrimethoxysilane (APTMS)-ITO show average diameters of 257 ± 108 and 72 ± 20 nm as well as average heights of 40 and

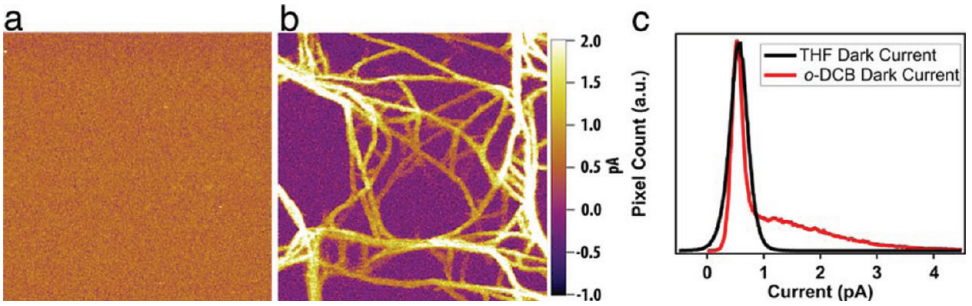

Figure 3. Dark current images collected at +1 V from (a) THF- and (b) *o*-DCB-cast films and (c) corresponding dark current distributions: THF- (black line) and *o*-DCB-cast (red line) films. Image sizes are 2 μm × 2 μm.

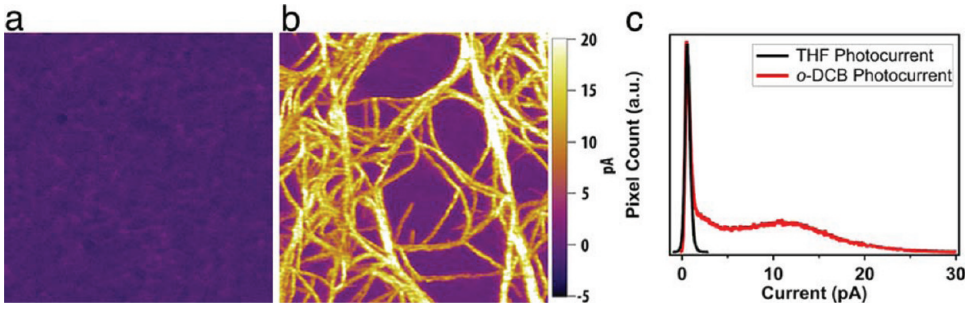

Figure 4. Photocurrent images collected at 0 V from (a) THF- and (b) *o*-DCB-cast films and corresponding photocurrent distributions (c): THF- (black line) and *o*-DCB-cast (red line) films. Image sizes are 2 μm × 2 μm.

6 nm, respectively, while fibers have an average width of 65 ± 23 and 88 ± 26 nm, respectively. It has been previously reported that, because P3HT is more soluble in THF than C_{61} (~2.3 mg/mL *versus* 0 mg/mL),[53,54] it is possible that the PCB unit of this polymer aggregates into a micellar core, leaving the P3HT tails exposed to provide colloidal stability in this solvent (Figure 2c). These micelles formed in solution are then transferred onto the film when the solution is cast and the end effect is the self-assembly of nanospheres on the film. C_{61} shows much higher solubility in *o*-DCB than P3HT (107 mg/mL *versus* 20 mg/mL). This difference in solubility drives the P3HT portions to aggregate together. The high boiling point of *o*-DCB results in a slow drying process during film preparation, thus it allows for crystallization of a P3HT core with a shell of PCBs surrounding them (Figure 2f), where the end effect is the formation of fibers that can span greater than 10 μm in length. These topography images confirm that casting PCB-c-P3HT from different solvents changes the self-assembled nanostructures formed in the film, and although substrates affect the dimensions of nanospheres and fibers, they do not affect the types of nanostructures formed.

The electrical properties of these different self-assembled nanostructures can be probed by c-AFM (Figure 3). In the THF-cast film scanned at +1 V applied bias in the dark, the surface is featureless and the dark current histogram shows a Gaussian distribution of currents centered at 0.6 pA (fwhm = 0.7 pA), which signifies that there are no preferential pathways for current to travel at this applied bias. The dark current image of *o*-DCB-cast film collected at +1 V comprises high current networks. The average width of these high current wires is 73 ± 32 nm. When looking at the current histogram, there is a Gaussian centered at 0.5 pA (fwhm = 0.3 pA), which is attributed to the background current, but there is also a tail of currents that extends to about 4.5 pA, which is attributed to the current gathered from the nanowires. This observation signifies that the nanowires are a pathway for injected charges to travel as opposed to the nanospheres, which show no conduction pathways.

Next, using pc-AFM, we probe whether charge generation would be possible in these nanostructures and what effect self-assembly has on photocharge generation in PCB-c-P3HT (Figure 4). Due to the inverted device architecture utilized in this study, the gold-coated probe, having a work function of 5.0 eV, collects photogenerated holes and the APTMS-ITO bottom contact, having a work function of 4.3 eV, collects photogenerated electrons.[38,55] The photocurrent image from the THF-cast film shows very low current with an average current of 1 pA. Several circular shape domains with a diameter of 87 ± 20 nm, similar to the features observed in Figure 2, have almost no photocurrent. In contrast, the fibers of PCB-c-P3HT from the *o*-DCB-cast film show remarkably high photocurrent when compared to the background, and from the histogram, we can make out two Gaussian distributions of photocurrent. The narrow Gaussian with lower photocurrent centered at 1 pA (fwhm = 0.8 pA)

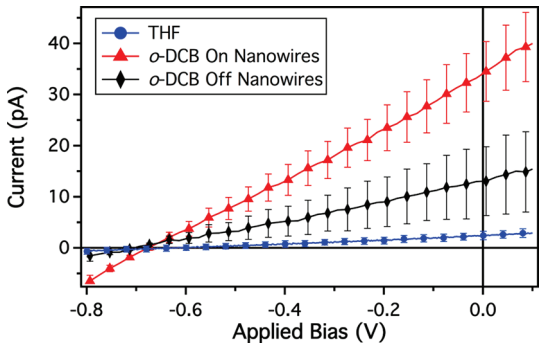

Figure 5. Average *I*−*V* curves of THF- and *o*-DCB-cast films collected under white light illumination: THF-cast film (blue circles), *o*-DCB-cast film collected on fibers (red triangle), and *o*-DCB-cast film collected off fibers (black diamond).

corresponds to the background current, while the broader Gaussian with higher photocurrent centered at 12 pA corresponds to the photocurrent on the nanowires.

The photocharge generation and transport of these different nanostructures can be revealed in greater detail through nano current−voltage (*I*−*V*) curves (Figure 5). The average nano *I*−*V* curve for the THF-cast film gives a short-circuit current (I_{SC}) of 2.4 pA and an average open-circuit voltage (V_{OC}) of −0.63 V. The average nano *I*−*V* characteristics of the *o*-DCB-cast film are collected from the flat regions as well as atop of the wires. The nano *I*−*V* curve collected from the flat regions shows an I_{SC} and V_{OC} of 13 pA and −0.69 V, respectively, whereas the nano *I*−*V* curve collected atop the fibers shows a I_{SC} and V_{OC} of 35 pA and −0.67 V, respectively. Using an estimation of contact area of our gold AFM probe to be 110 nm^2, the short-circuit current densities (J_{SC}) are calculated to be 2180, 11820, and 31820 mA/cm^2 for THF-cast films, flat region in *o*-DCB-cast films, and atop wires in *o*-DCB-cast films, respectively.[44] These observations indicate that charge generation and collection are much more efficient in film containing wires, perhaps due to the wires acting as a percolation network for electron transport. It should be noted that the difference in I_{SC} when scanning compared to collecting nano *I*−*V* measurements is due to the increase in the contact force and therefore contact area and tip−sample interaction when collecting nano *I*−*V* curves. This increase in contact area increases the effective volume of the sample probed, and better tip−sample contact reduces the charge collection barrier leading to an increase in measured photocurrent.

To further understand the formation of these fiber-like domains, films of PCB-c-P3HT with additional PCBM are cast from *o*-DCB and their photocurrent images are shown in Figure 6. In as-cast films (Figure 6a−c), additional PCBM allows the wires to increasingly pack and aggregate together to form "bundles" of wires (proposed self-assembly can be

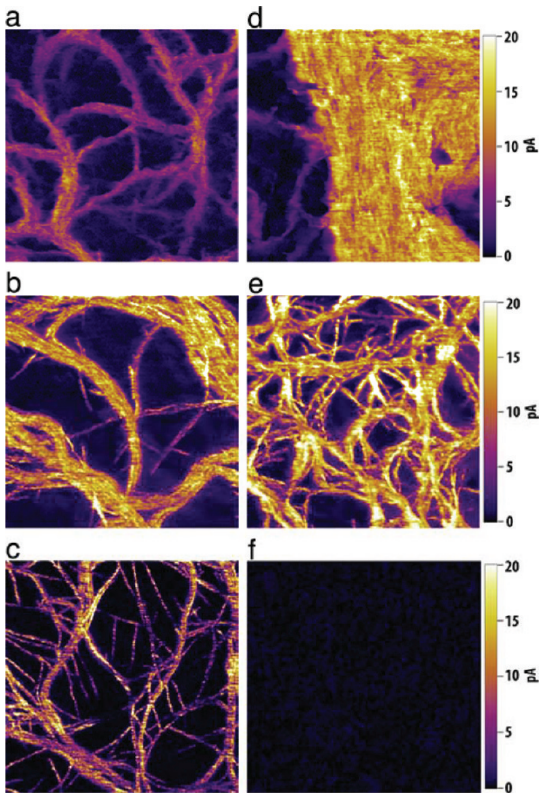

Figure 6. Photocurrent images of as-cast (a−c) and 110 °C annealed (d−f) *o*-DCB-cast film with 45.5% (a,d), 47.9% (b,e), and 66.5% (c,f) of C_{61} in PCB-c-P3HT solution. Image sizes are 2 μm × 2 μm.

seen in Supporting Information). In Figure 6b, individual wires can be resolved within the bundles. The widths of these nanowire bundles for the as-cast PCB-c-P3HT films with additional PCBM bringing the percent of C_{61} in the solution to 45.5, 47.9, and 66.5% are 162 ± 54, 195 ± 82, and 91 ± 45 nm, respectively. For as-cast films, wire bundling reaches its maximum in the PCB-c-P3HT film with 47.9% of C_{61} and further addition of PCBM causes wire coalescence. Subsequent films annealed for 10 min at 110 °C (Figure 6d−f) show drastic changes in nanoscale morphology. The widths of the wire bundles for the annealed PCB-c-P3HT films with 45.5 and 47.9% of C_{61} are 1277 ± 835 and 171 ± 70 nm, respectively, while the annealed PCB-c-P3HT film with 66.5% of C_{61} no longer shows wires at all. The annealed PCB-c-P3HT film with 47.9% of C_{61} shows massive bundling, which is not seen in the as-cast film, but annealing of PCB-c-P3HT with greater additions of PCBM causes thinner bundling until wires disappear altogether (Figure 6f). The formation of wire bundles and the increase in the bundle diameter with thermal annealing perhaps stem from the fact that fullerenes have a strong tendency to crystallize.

The *I*−*V* characteristics of *o*-DCB-cast PCB-c-P3HT films processed with additional PCBM are shown in Figure 7. In the as-cast films, the I_{SC} values for the PCB-c-P3HT films with 45.5, 47.9, and 66.5% of C_{61} are

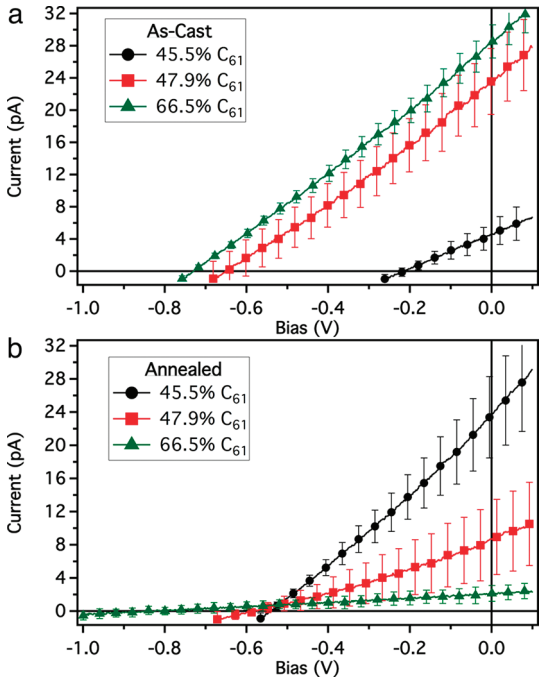

Figure 7. Average *I*−*V* curves of (a) as-cast and (b) annealed PCB-c-P3HT *o*-DCB-cast films with added PCBM collected under white light illumination on fiber-like domains: 45.5% of C_{61} (black circles), 47.9% of C_{61} (red squares), and 66.5% of C_{61} (green triangles).

5, 23, and 28 pA, respectively, while the V_{OC} values are −0.2, −0.65, and −0.73 V, respectively. Annealing of the films causes the I_{SC} values for the PCB-c-P3HT film with 45.5, 47.9, and 66.5% of C_{61} to change to 24, 8.7, and 2.1 pA, respectively, while the V_{OC} values change to −0.54, −0.59, and −0.84 V, respectively. These changes in I_{SC} correlate well to the degree of fiber bundles seen in the corresponding photocurrent images and are exemplified by the annealed film with 66.5% C_{61} showing the lowest I_{SC} when nanowires are nonexistent. The changes in V_{OC} in the films can also be attributed to changes in morphology, where it is well-known that casting and processing conditions affect the V_{OC}.[56−58] In as-cast films, small additions of PCBM disrupts the electron transport networks of the PCB-c-P3HT nanowires giving rise to the low V_{OC}, while further additions contribute to nanowire formation, which appear as nanowire bundles. Annealing of these films can help to induce similar quasi-Fermi level of the active layers through morphology, which contributes to similar V_{OC} values for all devices.

Next, we investigate whether PCB-c-P3HT can function as a molecular additive for P3HT:PCBM films using pc-AFM (Figure 8). Molecular additives or surfactants[9,11] are different from solvent additives[6−8] because they remain in the film whereas most of solvent additives evaporate during the film drying process. Molecular additives or surfactants have been shown to improve BHJ solar cell performance.[11,48] In P3HT:PCBM films, prepared with and without PCB-c-P3HT, both samples show similar fiber-like structures with high photocurrent; however, the P3HT:PCBM samples prepared with PCB-c-P3HT show a more than 100% higher photocurrent than that of P3HT:PCBM. As seen in the average nano *I*−*V* curves collected from as-cast and annealed P3HT:PCBM with and without additive, addition of PCB-c-P3HT increases the I_{SC} and V_{OC} of P3HT:PCBM films. The as-cast film's I_{SC} and V_{OC} increase from 13.9 pA and −0.35 V to 30.3 pA and −0.48 V, respectively. Thermal annealing of the PCB-c-P3HT:P3HT:PCBM film further doubles the I_{SC} from 22.7 to 47.7 pA, whereas the V_{OC} changes slightly from −0.44 to −0.49 V. Interestingly, the as-cast film with PCB-c-P3HT additive shows higher I_{SC} and V_{OC} characteristics with respect to the annealed film without the additive. This shows that PCB-c-P3HT is a suitable molecular additive to control the nanoscale morphology in BHJ P3HT:PCBM devices.

The ability of the nanowires of PCB-c-P3HT to conduct charge better than the nanospheres is attributed to the nanomorphology. When photocurrent is generated in the nanospheres, holes are located on the outer P3HT shell of the micelle nanospheres and it is difficult for the holes to travel to the anode because there is insufficient ordering of the P3HT tails. The electrons are further isolated from any percolated pathways because each C_{61} micelle core is separate from other micelle cores. This limits the mobility, as was discussed earlier, but with the combination of both holes and electrons being localized on the nanospheres where they originate, the probability of photoinduced charge recombination is high.

In contrast, in the *o*-DCB-cast film, the crystallization of the P3HT portion of the dyad in the core of the wires and the shell of methanofullerene around them can allow for the PCB and P3HT domains of the dyad to be able to transport charges.[59] The crystallization of the P3HT allows for increased mobility and long-range order and further elucidates why higher dark current is seen on the fibers. High photocurrent is also seen in the nanowires with respect to the nanospheres, as both P3HT and PCB segments are oriented to provide a well-defined pathway for photogenerated holes and electrons, respectively, to transport to the anode and cathode, respectively. This could explain the increase in I_{SC} from the background in nano *I*−*V* measurements of the *o*-DCB-cast film when compared to that of the nanospheres from the THF-cast film. The background of the *o*-DCB-cast film is penetrated by what might be considered a charge transporting nanowire "highway", which can decrease the amount of charges lost in that layer due to recombination causing an increase in the photocurrent measured in the background morphology.

The bundling of wires in PCB-c-P3HT films processed from *o*-DCB with additional PCBM further supports the proposed structure of PCB-c-P3HT wires. The additional PCBM acts as a sort of glue for aggregation of the wires and, at certain concentration, provides

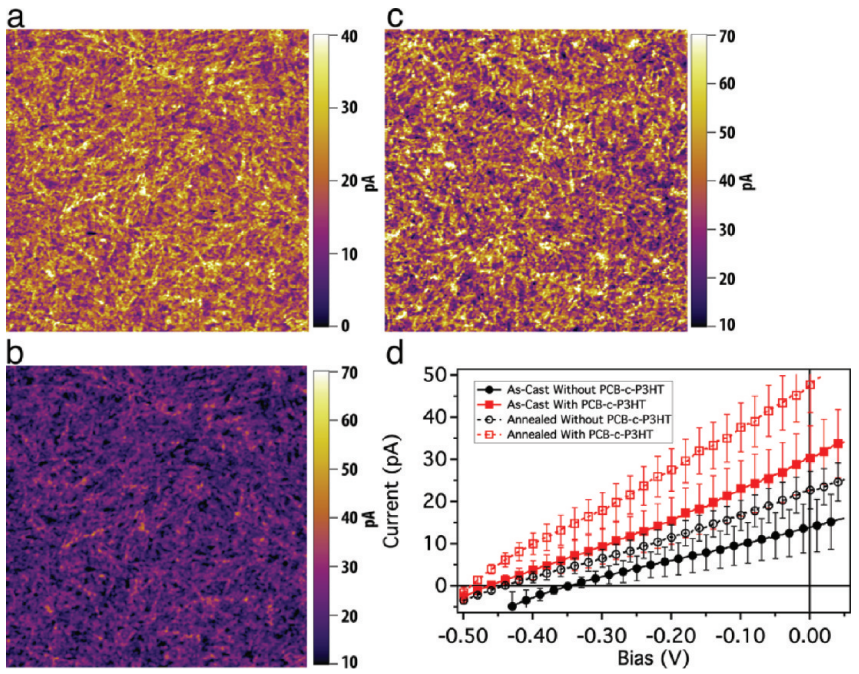

Figure 8. Photocurrent images collected at 0 V under white light illumination of annealed P3HT:PCBM films (a,b) without and (c) with PCB-c-P3HT as a molecular additive and corresponding average nano white light *I*−*V* curves (d): as-cast (solid lines with solid markers) and annealed (dashed lines with open markers) *o*-DCB-cast P3HT:PCBM films without (black circles) and with (red squares) added PCB-c-P3HT. Photocurrent image of annealed P3HT:PCBM film without PCB-c-P3HT (b) is shown with the same current scale as that with PCB-c-P3HT for better comparison. Images sizes are 5 μm × 5 μm.

percolation path to transport electrons,[60] thus, leading to higher J_{SC} (see Supporting Information Supplemental 3 for a schematic drawing). Though this bundling occurs at moderate PCBM concentrations, at low concentrations, the PCBM seems to interfere with the packing of PCB-c-P3HT wires causing a low J_{SC} relative to pristine PCB-c-P3HT fibers. This can be overcome by thermal annealing, which drastically increases the bundling of wires at low PCBM concentrations while dissociating fibers into an amorphous layer with no charge generation or transportation pathways at higher PCBM concentrations. The low injected and photocurrent observed from the THF-cast film data is consistent with previous studies[49] that, in THF-cast PCB-c-P3HT films, the PCB units aggregate into a nanosphere structure with the P3HT chains extending outward, while the fibrous PCB-c-P3HT structures in *o*-DCB-cast films P3HT chains crystallize to form a core, which is surrounded by a monolayer of C_{61} moieties. The low current is due to the lack of percolation pathway to transport charges in the micelle morphology.

In addition to the nanoscale formation, we show that PCB-c-P3HT acts as a suitable molecular additive to P3HT:PCBM BHJ's by increasing both the I_{SC} and V_{OC}. Thermal annealing can be used to improve nanoscale formation in films, but as we can see when comparing the annealed nano *I*−*V* curve without additive with that of the as-cast film with additive in Figure 8, addition of PCB-c-P3HT increases the *I*−*V* characteristics more than that of annealing. Annealing of P3HT:PCBM film with PCB-c-P3HT additive further increases the nano *I*−*V* characteristics of the film, which shows that addition of the molecular additive enhances the self-assembly of the P3HT:PCBM BHJ without the need for thermal annealing.

CONCLUSIONS

In summary, we have studied the nanoscale electronic and optoelectronic properties of two distinct self-assembled nanostructures of a PCB-c-P3HT dyad using c-AFM and pc-AFM. In contrast to previous studies of physically mixed polymer:fullerene blends, the covalent link between the methanofullerene and the P3HT block creates well-defined interfaces of phases in thin films. The pc-AFM study of the self-assemblies of PCB-c-P3HT provides direct evidence at the nanoscale level of how the structure and morphology of the polymer/fullerene interface determines the photoinduced charge generation and the subsequent charge migration to electrodes. The nanospheres formed from THF solution show low dark current and photocurrent because both the PCB and P3HT portions of the dyad are isolated from the rest of the film, which decreases mobility and increases the recombination probability of charges. On the other hand, the crystallization of the P3HT core and alignment of the PCB of the dyad in the wires from the *o*-DCB-cast film allows for high mobility and delocalization of charges, giving high dark current and photocurrent. This is supported by PCB-c-P3HT films created with additional PCBM

where the free PCBM can allow for bundling of the wires but can also inhibit wire formation under annealing conditions. We have also shown that PCB-c-P3HT can be used as a suitable molecular additive in P3HT:PCBM devices. This study underscores the importance of molecular design and morphological control of phase separation for developing highly efficient polymer:fullerene BHJ photovoltaics.

METHODS

The P3HT precursor used in the synthesis of PCB-c-P3HT contained an average degree of polymerization of 24 (M_n = 4000 g/mol and PDI = 1.4). The change in nanostructure formation of a PCB-c-P3HT film is due to the difference in solubility of each component of the dyad.[49] To form different nanostructures, solutions of 2 mg/mL in THF and 1 mg/mL in *o*-DCB of PCB-c-P3HT were prepared in a glovebox and sonicated overnight at room temperature.[49]

Films of PCB-c-P3HT were prepared by drop casting the solutions under nitrogen atmosphere. Silicon, unmodified transparent ITO, and ITO modified with a self-assembled monolayer of APTMS, which has a work function of 4.30 eV[38] (similar to the work function of aluminum), were used as substrates. APTMS-ITO was prepared according to previously reported procedures.[38,39,61] Cleaned ITO was activated by sonicating in $H_2O/NH_3/H_2O_2$ (5:1:1 by volume) solution for 15 min and then soaked in 1% APTMS in methanol for an hour to allow APTMS to self-assemble onto ITO. THF- and *o*-DCB-cast films were left to dry under nitrogen atmosphere for 1 and 3 days, respectively, before measurements were taken because of the high boiling point of *o*-DCB. Further, three *o*-DCB solutions of PCB-c-P3HT with additional PCBM were created by adding 28.5, 57, and 144 μg of PCBM to 100 μL of 1 mg/mL PCB-c-P3HT, bringing the total percent of C_{61} in the solution to 45.5, 47.9, and 66.5%. Resulting films were cast on APTMS-ITO substrates with the methods stated. Subsequent PCB-c-P3HT films with 45.5, 47.9, and 66.5% of C_{61} were prepared and annealed for 10 min at 110 °C. To test the effect of PCB-c-P3HT as a molecular additive, 50 μL of a 1:1 by weight ratio of P3HT:PCBM in a 5 wt % *o*-DCB solution was prepared with 10 μL of 1 mg/mL of PCB-c-P3HT added to it. Films of this solution were spin-cast at 600 rpm on APTMS-ITO. After measurements were preformed on as-cast films, the films were annealed at 110 °C for 10 min inside a nitrogen glovebox. Thicknesses of all films are reported in the Supporting Information.

After the films were cast and dried, the electrical and optoelectrical properties of PCB-c-P3HT were examined. To elucidate these properties, we utilized t-AFM, c-AFM, and pc-AFM, using an Asylum Research MFP-3D AFM sitting atop an inverted optical microscope (Olympus, IX71) as described in previous publications.[5,38,39] In pc-AFM measurements, light from a xenon lamp source is coupled into an inverted optical microscope through the use of a fiber optic cable and focused with an objective into a spot size ~160 μm in diameter. Power from the spot size was measured to be ~300 suns (~ 30 W/cm^2). All measurements were performed using an airtight sample holder continuously flushed with nitrogen to prevent exposure of the sample to moisture and oxygen. Silicon probes with a resonant frequency of 62 kHz and spring constant of 3 N/m were used for t-AFM measurements (Vista Probes), and gold-coated AFM probes with a resonant frequency of 13 kHz and a force constant of 0.2 N/m were used for c-AFM and pc-AFM measurements (Budget Sensors). The c-AFM scans were collected without illumination and at a constant bias applied to the substrate with current recorded by the internal preamplifier (Asylum Research ORCA head model). In the c-AFM mode, charges are injected from either the substrate or the AFM probe through the active layer. This allows for surface mapping of percolated pathways for current to travel through a film. In pc-AFM mode, scans are collected in the same manner as c-AFM but the film is scanned under short-circuit conditions (no applied bias) and the sample is illuminated from below through the transparent APTMS-ITO electrode. In both modes, surface topography and injected current or photocurrent images are collected simultaneously. Nano $I-V$ curves were collected either under dark or white light conditions and are averages of at least 25 individual locations. In nano $I-V$ measurements, the metal probe was positioned at one location and biases were scanned from −5 to +5 V while current was collected.

Conflict of Interest: The authors declare no competing financial interest.

Acknowledgment. We thank the NSF Special Creativity Award for the financial support of this work. F.W. and M.W. thank the DOE-BES (DE-FG02-08ER46535) for support. M.W. thanks the NSERC of Canada for a Postdoctoral Fellowship.

Supporting Information Available: Additional $I-V$ curves of THF- and *o*-DCB-cast films, proposed self-assembly model of nanowire bundles, and film thicknesses. This material is available free of charge *via* the Internet at http://pubs.acs.org.

REFERENCES AND NOTES

1. Krebs, F. C. Fabrication and Processing of Polymer Solar Cells: A Review of Printing and Coating Techniques. *Sol. Energy Mater. Sol. Cells* **2009**, *93*, 394–412.
2. Yu, G.; Gao, J.; Hummelen, J. C.; Wudl, F.; Heeger, A. J. Polymer Photovoltaic Cells: Enhanced Efficiencies *via* a Network of Internal Donor−Acceptor Heterojunctions. *Science* **1995**, *270*, 1789–1791.
3. Peet, J.; Heeger, A. J.; Bazan, G. C. "Plastic" Solar Cells: Self-Assembly of Bulk Heterojunction Nanomaterials by Spontaneous Phase Separation. *Acc. Chem. Res.* **2009**, *42*, 1700–1708.
4. Peet, J.; Senatore, M. L.; Heeger, A. J.; Bazan, G. C. The Role of Processing in the Fabrication and Optimization of Plastic Solar Cells. *Adv. Mater.* **2009**, *21*, 1521–1527.
5. Mark, D.; Peet, J.; Nguyen, T.-Q. Nanoscale Charge Transport and Internal Structure of Bulk Heterojunction Conjugated Polymer/Fullerene Solar Cells by Scanning Probe Microscopy. *J. Phys. Chem. C* **2008**, *112*, 7241–7249.
6. Moon, J. S.; Takacs, C. J.; Cho, S.; Coffin, R. C.; Kim, H.; Bazan, G. C.; Heeger, A. J. Effect of Processing Additive on the Nanomorphology of a Bulk Heterojunction Material. *Nano Lett.* **2010**, *10*, 4005–4008.
7. Peet, J.; Kim, J. Y.; Coates, N. E.; Ma, W. L.; Moses, D.; Heeger, A. J.; Bazan, G. C. Efficiency Enhancement in Low-Bandgap Polymer Solar Cells by Processing with Alkane Dithiols. *Nat. Chem.* **2007**, *6*, 497–500.
8. Lee, J. K.; Ma, W. L.; Brabec, C. J.; Yuen, J.; Moon, J. S.; Kim, J. Y.; Lee, K.; Bazan, G. C.; Heeger, A. J. Processing Additives for Improved Efficiency from Bulk Heterojunction Solar Cells. *J. Am. Chem. Soc.* **2008**, *130*, 3619–3623.
9. Dante, M.; Yang, C.; Walker, B.; Wudl, F.; Nguyen, T.-Q. Self-Assembly and Charge-Transport Properties of a Polythiophene−Fullerene Triblock Copolymer. *Adv. Mater.* **2010**, *22*, 1835–1839.
10. Chu, C.-C.; Raffy, G.; Ray, D.; Guerzo, A. D.; Kauffmann, B.; Wantz, G.; Hirsch, L.; Bassani, D. M. Self-Assembly of Supramolecular Fullerene Ribbons *via* Hydrogen-Bonding Interactions and Their Impact on Fullerene Electronic Interactions and Charge Carrier Mobility. *J. Am. Chem. Soc.* **2010**, *132*, 12717–12723.
11. Yang, C.; Lee, J. K.; Heeger, A. J.; Wudl, F. J. Well-Defined Donor−Acceptor Rod−Coil Diblock Copolymers Based on P3HT Containing C60: The Morphology and Role as a Surfactant in Bulk-Heterojunction Solar Cells. *Mater. Chem.* **2009**, *19*, 5416–5423.

12. Fernández, G.; Pérez, E. M.; Sánchez, L.; Martín, N. Self-Organization of Electroactive Materials: A Head-to-Tail Donor−Acceptor Supramolecular Polymer. *Angew. Chem., Int. Ed.* **2008**, *47*, 1094–1097.
13. Brettreich, M.; Burghardt, S.; Böttcher, C.; Bayerl, T.; Bayerl, S.; Hirsch, A. Globular Amphiphiles: Membrane-Forming Hexaadducts of C60. *Angew. Chem., Int. Ed.* **2000**, *39*, 1845–1848.
14. Nakanishi, T.; Shen, Y.; Wang, J.; Li, H.; Fernandes, P.; Yoshida, K.; Yagai, S.; Takeuchi, M.; Ariga, K.; Kurth, D. G.; *et al.* Superstructures and Superhydrophobic Property in Hierarchical Organized Architectures of Fullerenes Bearing Long Alkyl Tails. *J. Mater. Chem.* **2010**, *20*, 1253–1260.
15. Nakanishi, T.; Schmitt, W.; Michinobu, T.; Kurth, D. G.; Ariga, K. Hierarchical Supramolecular Fullerene Architectures with Controlled Dimensionality. *Chem. Commun.* **2006**, 5982–5984.
16. Guldi, D. M.; Zerbetto, F.; Georgakilas, V.; Prato, M. Ordering Fullerene Materials at Nanometer Dimensions. *Acc. Chem. Res.* **2005**, *38*, 38–43.
17. Cassell, A. M.; Asplund, C. L.; Tour, J. M. Self-Assembling Supramolecular Nanostructures from a C60 Derivative: Nanorods and Vesicles. *Angew. Chem., Int. Ed.* **1999**, *38*, 2403–2405.
18. Chu, C.-W.; Yang, H.; Hou, W.-J.; Huang, J.; Li, G.; Yang, Y. Control of the Nanoscale Crystallinity and Phase Separation in Polymer Solar Cells. *Appl. Phys. Lett.* **2008**, *92*, 1033061–1033063.
19. Chiu, M.-Y.; Jeng, U.-S.; Su, M.-S.; Wei, K.-H. Morphologies of Self-Organizing Regioregular Conjugated Polymer/Fullerene Aggregates in Thin Film Solar Cells. *Macromolecules* **2010**, *43*, 428–432.
20. Klop, E. A.; Lammers, M. XRD Study of the New Rigid-Rod Polymer Fibre PIPD. *Polymer* **1998**, *39*, 5987–5998.
21. Yang, X.; Loos, J.; Veenstra, S. C.; Verhees, W. J. H.; Wienk, M. M.; Kroon, J. M.; Michels, M. A. J.; Janssen, R. A. Nanoscale Morphology of High-Performance Polymer Solar Cells. *Nano. Lett.* **2005**, *5*, 579–583.
22. Matsuo, N.; Sato, Y.; Niinomi, T.; Soga, I.; Tanaka, H.; Nakamura, E. Columnar Structure in Bulk Heterojunction in Solution-Processable Three-Layered p-i-n Organic Photovoltaic Devices Using Tetrabenzoporphyrin Precursor and Silylmethyl[60]fullerene. *J. Am. Chem. Soc.* **2009**, *131*, 16048–16050.
23. Hoppe, H.; Niggemann, M.; Winder, C.; Kraut, J.; Hiesgen, R.; Hinsch, A.; Meissner, D.; Sariciftci, N. S. Nanoscale Morphology of Conjugated Polymer/Fullerene-Based Bulk-Heterojunction Solar Cells. *Adv. Funct. Mater.* **2004**, *14*, 1005–1011.
24. Grévin, B.; Rannou, P.; Payerne, R.; Pron, A.; Travers, J.-P. Scanning Tunneling Microscopy Investigations of Self-Organized Poly(3-hexylthiophene) Two-Dimensional Polycrystals. *Adv. Mater.* **2003**, *15*, 881–884.
25. Scharber, M. C.; Mühlbacher, D.; Koppe, M.; Denk, P.; Waldauf, C.; Heeger, A. J.; Brabec, C. J. Design Rules for Donors in Bulk-Heterojunction Solar Cells—Towards 10% Energy-Conversion Efficiency. *Adv. Mater.* **2006**, *18*, 789–794.
26. Walker, B.; Tamayo, A. B.; Dang, X.-D.; Zalar, P.; Seo, J. H.; Garcia, A.; Tantiwiwat, M.; Nguyen, T.-Q. Nanoscale Phase Separation and High Photovoltaic Efficiency in Solution-Processed, Small-Molecule Bulk Heterojunction Solar Cells. *Adv. Funct. Mater.* **2009**, *19*, 3063–3069.
27. Li, G.; Shrotriya, V.; Yao, Y.; Huang, J.; Yang, Y. Manipulating Regioregular Poly(3-hexylthiophene):[6,6]-Phenyl-C61-butyric Acid Methyl Ester Blends—Route towards High Efficiency Polymer Solar Cells. *J. Mater. Chem.* **2007**, *17*, 3126–3140.
28. Villers, B. T. d.; Tassone, C. J.; Tolbert, S. H.; Schwartz, B. J. Improving the Reproducibility of P3HT:PCBM Solar Cells by Controlling the PCBM/ Cathode Interface. *J. Phys. Chem. C* **2009**, *113*, 18978–18982.
29. Yip, H.-L.; Hau, S. K.; Baek, N. S.; Ma, H.; Jen, A. K.-Y. Polymer Solar Cells That Use Self-Assembled-Monolayer- Modified ZnO/Metals as Cathodes. *Adv. Mater.* **2008**, *20*, 2376–2382.
30. Kim, C. S.; Kim, J. B.; Lee, S. S.; Kim, Y. S.; Loo, Y.-L. Sequence of Annealing Polymer Photoactive Layer Influences the Air Stability of Inverted Solar Cells. *Org. Electron.* **2009**, *10*, 1483–1488.
31. Luria, J. L.; Schwarz, K. A.; Jaquith, M. J.; Hennig, R. G.; Marohn, J. A. Spectroscopic Characterization of Charged Defects in Polycrystalline Pentacene by Time- and Wavelength- Resolved Electric Force Microscopy. *Adv. Mater.* **2010**, *23*, 624–628.
32. Douhéret, O.; Swinnen, A.; Bertho, S.; Haeldermans, I.; D'Haen, J.; D'Olieslaeger, M.; Vanderzande, D.; Manca, J. V. High-Resolution Morphological and Electrical Characterisation of Organic Bulk Heterojunction Solar Cells by Scanning Probe Microscopy. *Prog. Photovoltaics* **2007**, *15*, 713–726.
33. Ellison, D. J.; Lee, B.; Podzorov, V.; Frisbie, C. D. Surface Potential Mapping of SAM-Functionalized Organic Semiconductors by Kelvin Probe Force Microscopy. *Adv. Mater.* **2010**, *23*, 502–507.
34. Spadafora, E. J.; Demadrille, R.; Ratier, B.; Grevin, B. Imaging the Carrier Photogeneration in Nanoscale Phase Segregated Organic Heterojunctions by Kelvin Probe Force Microscopy. *Nano Lett.* **2010**, *10*, 3337–3342.
35. Reid, O. G.; Munechika, K.; Ginger, D. S. Space Charge Limited Current Measurements on Conjugated Polymer Films Using Conductive Atomic Force Microscopy. *Nano Lett.* **2008**, *8*, 1602–1609.
36. Douheret, O.; Lutsen, L.; Swinnen, A.; Breselge, M.; Vandewal, K.; Goris, L.; Manca, J. Nanoscale Electrical Characterization of Organic Photovoltaic Blends by Conductive Atomic Force Microscopy. *Appl. Phys. Lett.* **2006**, *89*, 0321071–0321073.
37. Kelley, T. W.; Granstrom, E.; Frisbie, C. D. Conducting Probe Atomic Force Microscopy: A Characterization Tool for Molecular Electronics. *Adv. Mater.* **1999**, *11*, 261.
38. Dang, X.-D.; Tamayo, A. B.; Seo, J.; Hoven, C. V.; Walker, B.; Nguyen, T.-Q. Nanostructure and Optoelectronic Characterization of Small Molecule Bulk Heterojunction Solar Cells by Photoconductive Atomic Force Microscopy. *Adv. Funct. Mater.* **2010**, *20*, 3314–3321.
39. Dang, X.-D.; Mikhailovsky, A.; Nguyen, T.-Q. Measurement of Nanoscale External Quantum Efficiency of Conjugated Polymer:Fullerene Solar Cells by Photoconductive Atomic Force Microscopy. *Appl. Phys. Lett.* **2010**, *97*, 1133031–1133033.
40. Pingree, L. S. C.; Reid, O. G.; Ginger, D. S. Imaging the Evolution of Nanoscale Photocurrent Collection and Transport Networks during Annealing of Polythiophene/Fullerene Solar Cells. *Nano Lett.* **2009**, *9*, 2946–2952.
41. Coffrey, D. C.; Reid, O. G.; Rodovsky, D. B.; Bartholomew, G. P.; Ginger, D. S. Mapping Local Photocurrents in Polymer/Fullerene Solar Cells with Photoconductive Atomic Force Microscopy. *Nano Lett.* **2007**, *7*, 738–744.
42. Bull, T. A.; Pingree, L. S. C.; Jenekhe, S. A.; Ginger, D. S.; Luscombe, C. K. The Role of Mesoscopic PCBM Crystallites in Solvent Vapor Annealed Copolymer Solar Cells. *ACS Nano* **2009**, *3*, 627–636.
43. Groves, C.; Reid, O. G.; Ginger, D. S. Heterogeneity in Polymer Solar Cells: Local Morphology and Performance in Organic Photovoltaics Studied with Scanning Probe Microscopy. *Acc. Chem. Res.* **2010**, *43*, 612–620.
44. Guide, M.; Dang, X.-D.; Nguyen, T.-Q. Nanoscale Characterization of Tetrabenzoporphyrin and Fullerene-Based Solar Cells by Photoconductive Atomic Force Microscopy. *Adv. Mater.* **2011**, *23*, 2313–2319.
45. Campoy-Quiles, M.; Ferenczi, T.; Agostinelli, T.; Etchegoin, P. G.; Kim, Y.; Anthopoulos, T. D.; Stavrinou, P. N.; Bradley, D. D. C.; Nelson, J. Morphology Evolution *via* Self-Organization and Lateral and Vertical Diffusion in Polymer: Fullerene Solar Cell Blends. *Nat. Mater.* **2008**, *7*, 158–164.
46. Thompson, B. C.; Fréchet, J. M. J. Polymer−Fullerene Composite Solar Cells. *Angew. Chem., Int. Ed.* **2008**, *47*, 58–77.
47. Treat, N. D.; Brady, M. A.; Smith, G.; Toney, M. F.; Kramer, E. J.; Hawker, C. J.; Chabinyc, M. L. Interdiffusion of PCBM and P3HT Reveals Miscibility in a Photovoltaically Active Blend. *Adv. Energy Mater.* **2011**, *1*, 82–89.

48. Lee, J. U.; Jung, J. W.; Emrick, T.; Russell, T. P.; Jo, W. H. Synthesis of C60-End Capped P3HT and Its Application for High Performance of P3HT/PCBM Bulk Heterojunction Solar Cells. *J. Mater. Chem.* **2010**, *20*, 3287–3294.
49. Wang, M.; Heeger, A. J.; Wudl, F. Self-Assembly of a Fullerene Poly(3-hexylthiophene) Dyad. *Small* **2011**, *7*, 298–301.
50. Schaller, R. D.; Lee, L. F.; Johnson, J. C.; Haber, L. F.; Saykally, R. J.; Vieceli, J.; Benjamin, I.; Nguyen, T.-Q.; Schwartz, B. J. The Nature of Interchain Excitations in Conjugated Polymers: Spatially-Varying Interfacial Solvatochromism of Annealed MEH-PPV Films Studied by Near-Field Scanning Optical Microscopy (NSOM). *J. Phys. Chem. B* **2002**, *106*, 9496–9505.
51. Shahid, M.; Ashraf, R. S.; Klemm, E.; Sensfuss, S. Synthesis and Properties of Novel Low-Band-Gap Thienopyrazine-Based Poly(heteroarylenevinylene)s. *Macromolecules* **2006** *39*, 7844–7853.
52. Miyanishi, S.; Zhang, Y.; Tajima, K; Hashimoto, K. Fullerene Attached All-Semiconducting Diblock Copolymers for Stable Single-Component Polymer Solar Cells. *Chem. Commun.* **2010**, *46*, 6723–6725.
53. Ruoff, R. S.; Tse, D. S.; Malhotra, R.; Lorents, D. C. Solubility of C60 in a Variety of Solvents. *J. Phys. Chem.* **1993**, *97*, 3379–3383.
54. Yamamoto, T.; Komarudin, D.; Arai, M.; Lee, B.-L.; Suganuma, H.; Asakawa, N.; Inoue, Y.; Kubota, K.; Sasaki, S.; Fukuda, T.; *et al.* Extensive Studies on π-Stacking of Poly(3-alkylthiophene-2,5-diyl)s and Poly(4-alkylthiazole-2,5-diyl)s by Optical Spectroscopy, NMR Analysis, Light Scattering Analysis, and X-ray Crystallography. *J. Am. Chem. Soc.* **1998**, *120*, 2047–2058.
55. Rider, D. A.; Worfolk, B. J.; Harris, K. D.; Lalany, A; Shahbazi, K; Fleischauer, M. D.; Brett, M. J.; Buriak, J. M. Stable Inverted Polymer/Fullerene Solar Cells Using a Cationic Polythiophene Modified PEDOT:PSS Cathodic Interface. *Adv. Funct. Mater.* **2010**, *20*, 2404–2415.
56. van Duren, J. K. J.; Yang, X.; Loos, J.; Bulle-Lieuwma, C. W. T.; Sieval, A. B.; Hummelen, J. C.; Janssen, R. A. J. Relating the Morphology of a Poly(*p*-phenylene vinylene)/Methanofullerene Blend to Bulk Heterojunction Solar Cell Performance. *Proc. SPIE* **2004**, *5215*, 99–110.
57. Singh, C. R.; Sommer, M.; Himmerlich, M.; Wicklein, A.; Krischok, S.; Thelakkat, M.; Hoppe, H. Morphology Controlled Open Circuit Voltage in Polymer Solar Cells. *Phys. Status Solidi RRL* **2011**, *5*, 247–249.
58. Reid, O. G.; Xin, H.; Jenekhe, S. A.; Ginger, D. S. Nanostructure Determines the Intensity-Dependence of Open-Circuit Voltage in Plastic Solar Cells. *J. Appl. Phys.* **2010**, *108*, 0843201–0843208.
59. Bottari, G.; Olea, D.; Gómez-Navarro, C.; Zamora, F.; Gómez-Herrero, J.; Torres, T. Highly Conductive Supramolecular Nanostructures of a Covalently Linked Phthalocyanine–C60 Fullerene Conjugate. *Angew. Chem., Int. Ed.* **2008**, *47*, 2026–2031.
60. Cates, N. C.; Gysel, R.; Beiley, Z.; Miller, C. E.; Toney, M. F.; Heeney, M.; McCulloch, I.; McGehee, M. D. Tuning the Properties of Polymer Bulk Heterojunction Solar Cells by Adjusting Fullerene Size to Control Intercalation. *Nano Lett.* **2009**, *9*, 4153–4157.
61. Sfez, R.; Peor, N.; Cohen, S. R.; Cohen, H.; Yitzchaik, S. *In Situ* SFM Study of 2D-Polyaniline Surface-Confined Enzymatic Polymerization. *J. Mater. Chem.* **2006**, *16*, 4044–4050.